This is the Pre-Published Version.
X. Huang, S. Link, A. Rodriguez, M. Thomsen, S. Olson, P. Ferkul, C. Fernandez-Pello (2019) *Transition from Opposed Flame Spread to Fuel Regression: Effect of Airflow, Pressure & Microgravity*, Proceedings of the Combustion Institute (37) 4117-26.
https://doi.org/10.1016/j.proci.2018.06.022

Transition from Opposed Flame Spread to Fuel Regression and Blow off: Effect of Flow, Atmosphere, and Microgravity

Xinyan Huang [a,b,*], Shmuel Link [b], Andy Rodriguez [b], Maria Thomsen [b], Sandra Olson [c], Paul Ferkul [c], Carlos Fernandez-Pello [b]

[a]*Department of Building Services Engineering, The Hong Kong Polytechnic University, Kowloon, Hong Kong*

[b]*Department of Mechanical Engineering, University of California, Berkeley, CA 94720, USA*

[c]*NASA Glenn Research Center at Lewis Field, Cleveland, OH, USA*

***Corresponding Author:** Xinyan Huang xy.huang@polyu.edu.hk

Abstract: The spread of flames over the surface of a solid combustible material in an opposed flow is different from the mass-burning (or fuel-regression) in a pool fire. However, the progress of the flame front over a solid fuel includes both flame-spread and fuel-regression, but the difference between these two processes has not been well clarified. In this work, experiments using cylindrical PMMA samples were conducted in normal gravity and in microgravity are analyzed to identify the transition from opposed flame-spread to fuel-regression under varying conditions, including sample size, opposed flow velocity, pressure, oxygen concentration, external radiation, and gravity level. For a thick rod in normal gravity, as the opposed flow increases to 50~100 cm/s, the flame can no longer spread over the fuel surface but stay in the recirculation zone downstream of the cylinder end surface, like a pool fire flame. The flame spread first transitions to fuel regression at a critical leading-edge regression angle of $\alpha \approx 45^{o}$, and then, flame blow-off occurs. Under large opposed flow velocity, a stable flat blue flame is formed floating above the rod end surface, because of vortex shedding. In microgravity at a low opposed flow (<10 cm/s), pure fuel-regression was not observed. This work aims to clarify the differences between the flame-spread and fuel-regression in the progress of the flame and provide a better understanding of blow-off phenomena on solid fuels.

Keywords: PMMA Rod; Burning; Regression Angle; Pressure; Extinction

1. Introduction

The spread of flames over the surface of the solid combustible material is a complex process involving the interaction between the solid phase (heat transfer, thermal decomposition, gasification) and the gas phase (transport, mixing, chemical kinetics) [1,2]. Flame spread is affected by external environmental conditions, such as external heating, flow, pressure, oxygen concentration, and gravity level [2–4]. The understanding of flame spread over solid fuel in the opposed flow has been greatly improved after continuous studies since the 1960s. de Ris [5] first provided a physical-based 2-D model to solve the opposed flame spread over a solid flat surface. Experimentally, Fernandez-Pello *et al.* [6,7] measured the downward flame spread over the thick PMMA sample for both a flat sheet and a rod under variable opposed flow velocity and O_2 concentration. They revealed a thermal regime in the low flow velocity/high oxygen concentration and a kinetic regime in high flow velocity/low oxygen concentration. Frey and T'ien [8] improved de Ris' model to simulate the opposed flame spread over thin fuels. Wichman [9] reviewed the historical development of the theory of opposed-flow flame spread. Microgravity experiments on the opposed flame spread [10–14] conducted in the space shuttle, and International Space Station (ISS) revealed different flame-spread

and extinction phenomena in low opposed flow velocity, which cannot be observed on Earth due to the strong buoyant flow.

Besides spreading over the fuel surface, a flame could also move due to the regression of fuel. However, the motion of flame due to fuel regression is clearly different from the flame-spread phenomenon. One example that illustrates the mass burning is the candle flame, where flame moves downward because of the regression of the candle top (both burning and dripping of wax), rather than flame spreading over the surface of the candle. The concept of fuel regression is widely used in the burning of a liquid pool fire [15], but not so much in the flame spread over solid. Several studies have noticed that there is a difference between opposed flame spread and mass burning (or fuel regression) [2]. Sibulkin and collaborators [16,17] showed that in the downward flame spread over a PMMA rod the top of rod within the flame formed a cone (see Fig. 1a). The shape of the cone became less sharp as the O_2 concentration was decreased and eventually became flat at the flame extinction. The numerical simulations by Kumar and T'ien [18] showed two stable flame-spread phenomena, the side-stabilized flame and wake flame. The latter occurred near extinction. Gollner *et al.* [19] noticed that the rate of flame spread and rate of burning had a very different trend with the inclination of fuel. Kobayashi *et al.* [20] showed that as the dripping flow increased, the rate of downward flame spread increased while the burning rate decreased. Carmignani *et al*. [21] found in the downward flame spread over a flat fuel, the angle of fuel wedge (burn angle) decreased with fuel thickness until it reached a limit of about 11º.

However, there are very limited studies comparing the difference between opposed flame spread and mass burning, and the transition between them. Nevertheless, it appears that there is a misuse or misinterpretation of these two very different phenomena. One example is for the interpretation of ASTM D2863-13 limiting oxygen test [22], that near extinction flame may no longer spread over the thick fuel, but it burns like a candle flame. Thus, the interpretation of the data may be questionable. In this work, the transition between opposed flame spread and mass burning is investigated experimentally with PMMA rods as the fuel. By introducing the regression angle, the influence of fuel size, opposed flow, pressure, O_2 concentration, external heating, and gravity level on this transition will be quantified.

2. Experimental Methods

The solid fuel samples used in all experiments are cast black PMMA cylinders with diameters of 0.32, 0.64, 0.95, and 1.27 cm and same length of 5.7 cm. The black PMMA is selected, instead of clear PMMA, to avoid the influence of in-depth radiation absorption and simplify the heat transfer analysis of the ignition under external radiation.

2.1. Normal gravity experiment

2.1.1. Ambient pressure tests

The experimental apparatus at normal gravity is similar to ASTM limiting oxygen test [22,23]. As illustrated in Fig. 1, it consisted of a small-scale cylindrical flow duct in which the cylindrical fuel sample was placed. The vertically oriented flow duct had an outer diameter of 75 mm and an inner diameter of 70 mm and is 254 mm long. Upstream from the flow duct, there was a flow mixing chamber, with inlets for pressurized air, O_2 and N_2. These pressurized gases were metered via sonic orifices that allowed for controlled flows of gas with a prescribed O_2 concentration between 16 and 27% at velocities up to 350 cm/s. The gas flows were mixed in a chamber and homogenized by a 50-mm long of borosilicate glass beads.

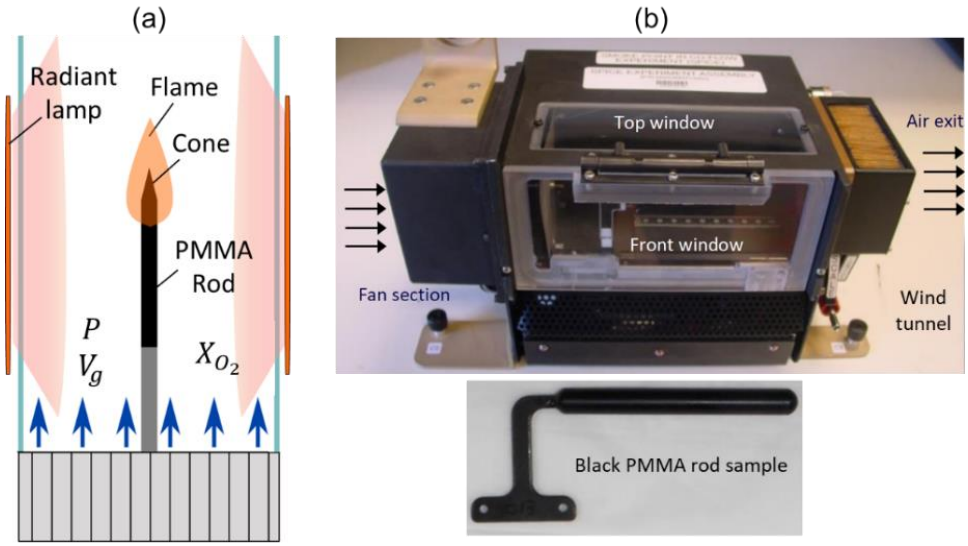

Fig. 1 (a) Schematic diagram of the experimental setup, and (b) microgravity test device and PMMA rod sample.

Facing the sample, outside of the quartz flow-duct were three halogen lamps (Ushio QIH120-500T/S, 12.7 cm long), equally spaced at 120° intervals. With the parabolic reflectors (Research Inc. 5236-05-A), they provided a uniform heat flux on the sample surface up to 35 kW/m^2, which was controlled by the supply power. For experiments under external radiation, the lamp was turned on along with the ignition. The ignition was achieved by using a small methane diffusion flame in still air. When the flame became robust, the designed opposed flow velocity and O_2 concentration were applied. A Nikon D300 camera was used to record the flame-spread process. A scale (precise up to 0.1 mg) is place below the sample holder to monitor the mass loss of selected experiments. All normal-gravity experiments were repeated at least three times to reduce the random error.

2.1.2. Reduced-pressure tests

The reduced-pressure experiment in normal gravity was conducted in a pressure chamber. Within the chamber, there is a tunnel with a 125-mm square cross-section and a 600-mm total length (see more detailed description in [24]). Reduced pressure ranging from 30 to 100 kPa were tested under the normal ambient O_2 level (21% O_2). The flowrates of dry compressed air were controlled by measuring the supply pressure and passed through precision control orifices and fixed to 10 and 20 cm/s. In the reduced pressure, the gas mass flow rate was also reduced to keep the same flow velocity. The ignition was achieved by a ceramic heater on the top of the sample under the given flow rate but under normal pressure. Once the flame was stabilized, the pressure was reduced, and the steady-state flame spread lasted from 6 to 12 min. Same Nikon D300 camera was used to record the flame-spread process. Each test conditions were also repeated at least three times.

2.2. Microgravity experiment

Microgravity flame spread tests were conducted in the BASS-II hardware placed inside the Microgravity Science Glovebox (MSG) in the ISS Destiny Lab. Photographs of the experiment are shown in Fig. 2. The BASS-II hardware provides a contained atmosphere in which it is possible to conduct fire safety experiments [10–13]. The test section of the duct had two orthogonal windows, allowing two cameras to record the experiment (Nikon D300 and Panasonic WV-CP654). The PMMA rod was manually ignited with a hot-wire igniter by the astronaut.

The flow was generated and controlled by a small fan at the upstream end of the duct. O_2 concentration was varied between 16% and 21%, and flow velocities were varied between 0.4 and 8 cm/s. Keeping the O_2 concentration of flow constant, each sample was ignited at a relatively elevated opposed flow velocity, and the steady-state flame spread was achieved within 1 min. Then, the opposed flow velocity was subsequently reduced until extinction was observed, pausing (about 30 s) along the way to allow for steady state flame spread at each new flow velocity. More detailed descriptions of the tests can be found in [10–13].

3. Results and discussions

After a strong ignition by the flame or ceramic heater, the rate of flame spread is observed to approach steady state within less than 1 min. For the measured mass-loss rate, it took 3~5 min to reach steady state, depending on the environmental condition. Once the mass-loss rate reaches steady state, the cone shape on the top surface of PMMA will not change.

3.1. Flame behaviors

Figure 2 shows the shapes of flame and cone for a 1.27-cm diameter PMMA rod under different opposed flow velocity, pressure, and gravity level. In normal gravity and ambient pressure (see Fig. 2(a) and see Video 1 in the supplemental material), as the opposed (upward) flow velocity (U_a) increases, both the flame length and cone height become shorter. At the same time, the observed flame-spread rate decreases. The flame width is larger than the diameter of the sample at $U_a < 75$ cm/s, while is almost equal to the sample diameter at $U_a > 75$ cm/s.

At high flow velocity ($U_a = 250$ cm/s), the flame becomes a flat sheet floating above the top of PMMA rod, i.e., within the stagnation (or recirculation) zone of the external flow. Figure 2(b) shows the evolution and top view of this flat flame where the occasional yellow flame tip occurs. Eventually, a pure blue flame sheet is formed at $U_a =$ 300 cm/s. This flat blue flame is very stable, and it can last for more than 15 min or until the burnout of fuel (see Video 2). On the other hand, the sample top surface is not completely flat, instead, it has a deeper regression towards the center (i.e., surface depression). Further increasing the flow velocity to 310 cm/s, the flame is blown off.

Decreasing the ambient pressure, the flame becomes blue (see Fig. 2(c) and Video 3), indicating a lower soot concentration in the flame or the soot moving away from hotter regions [25]. Under the same opposed flow, the flame width or the thickness of boundary layer increases. It is because the boundary layer grows as the density decreases and buoyancy effects become smaller at a lower pressure, as indicated by a smaller Grashof number. Compared to the normal pressure (Fig. 2a), both the flame height and the cone height are smaller at lower pressure.

In microgravity, the flame can spread in a much lower opposed flow velocity than in normal gravity because of the flame induced buoyant flow overcomes the forced flow (>30 cm/s). Figure 2(d) and Video 4 show the blue flame in microgravity which has a larger flame width and a shorter flame length. Moreover, as the opposed flow velocity decreases, the tip of the flame becomes open, and the length of the flame becomes even shorter than the length of the fuel cone.

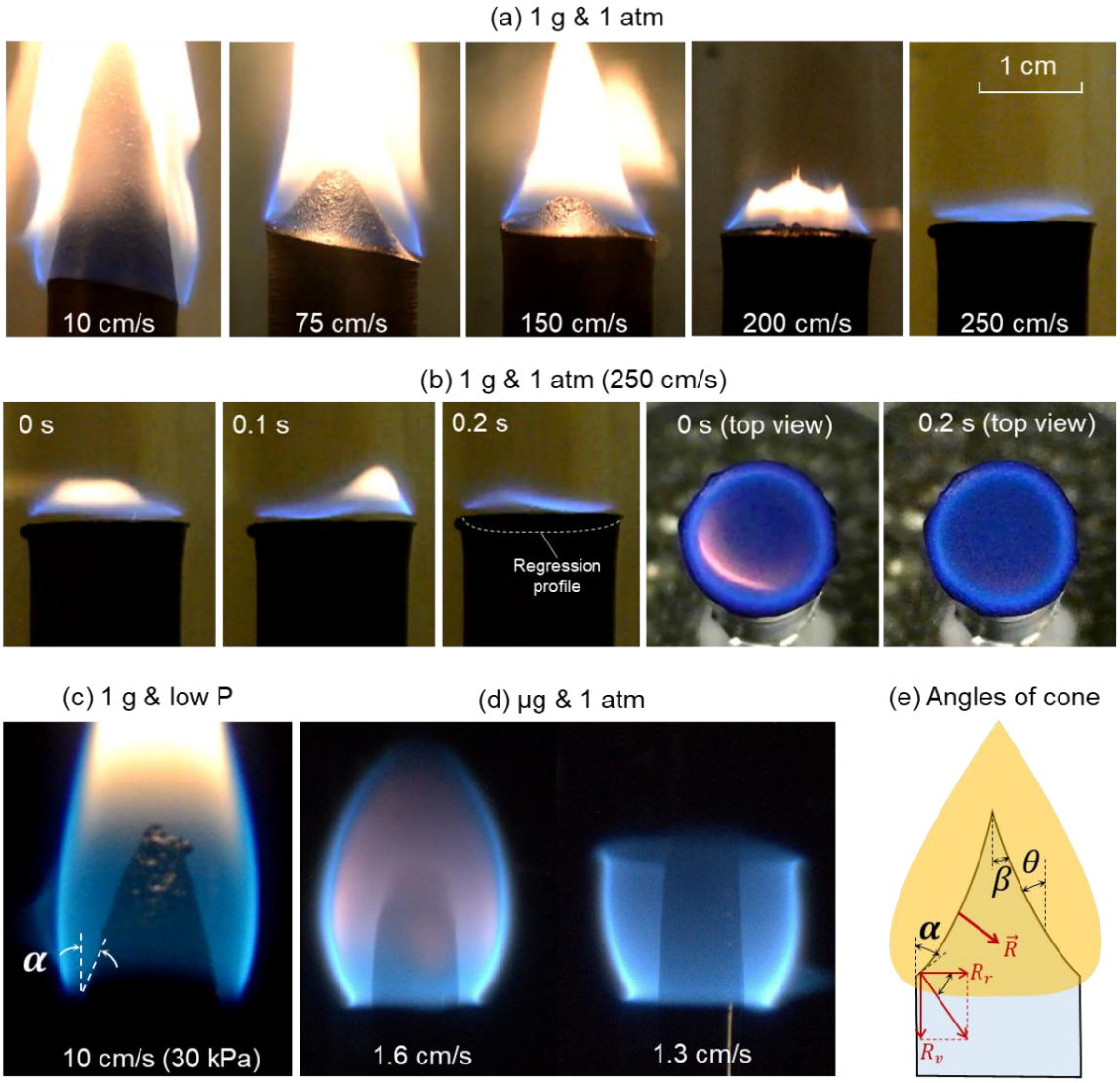

Fig. 2 Shape of flame with 1.27-cm diameter PMMA rod (O_2 = 21%) in (a) normal gravity (1g), (b) thin flame at opposed flow velocity of 250 cm/s, (c) reduced pressure at 1g, (d) microgravity and normal pressure, (e) angles in the cone, where α is the leading-edge regression angle, β is the cone angle, and θ is the average regression angle.

3.2. Flame structure

In this work, we analyze the difference between the opposed flame spread that occurs over the surface of a solid and mass burning (or fuel regression) that occurs downstream of the spreading flame front. Specifically, we aim to understand *the transition from the opposed flame spread to mass burning in a solid fuel.* It is hypothesized that this transition occurs when the external flow velocity exceeds the local laminar burning velocity, so that the flame stabilizes in the region behind the flame front where the flow velocity is smaller than the burning velocity.

This hypothesis assumes a triple flame in the flame leading edge, as illustrated in Fig. 3(a), where the partial premixed flaming is propagating against the opposed flow stabilizing the "bulk" diffusion flame [26]. In other words, when the opposed flow velocity is larger than the local laminar burning velocity, the premixed flame in the leading edge can no longer be sustained against the flow but move into the recirculation zone created behind the flame front.

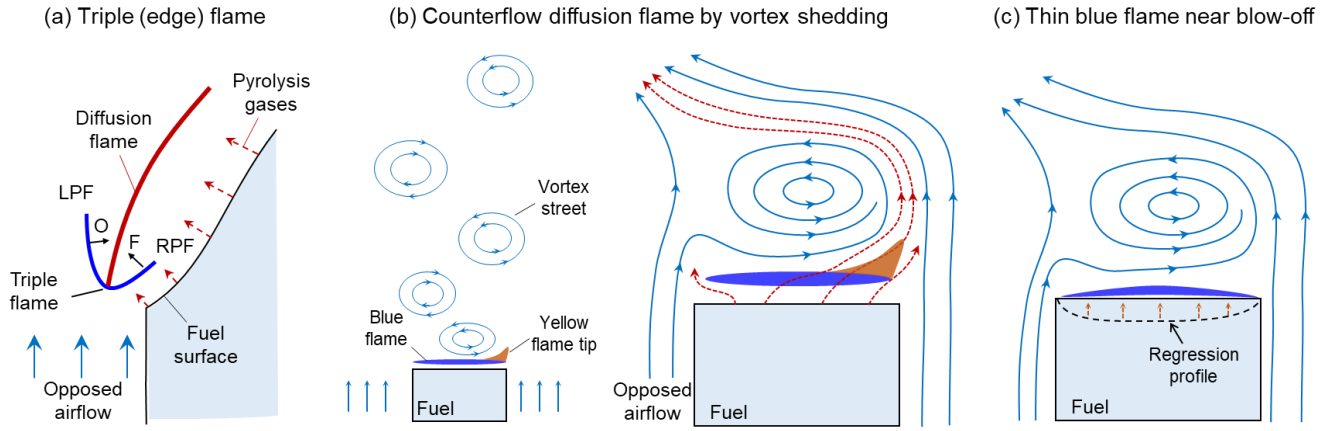

Fig. 3 Diagrams for (a) potential triple flame structure in the flame leading edge (lean premixed flame (LPF) + rich premixed flame (RPF) + diffusion flame), (b) counterflow-flame like thin diffusion flame under the large opposed airflow velocity, and (c) thin blue flame sheet near blow-off with top surface depression.

At the large opposed flow velocity, a counter-rotating vortex will be generated downstream above the fuel top surface, as illustrated in Fig. 3(b). Together with the uprising pyrolysis gas from solid fuel, a stagnation surface and a thin diffusion flame sheet are formed right downstream the fuel top surface. Such structure is similar to the classical pool fire or a counterflow diffusion flame, but it is less uniform which has a fuel-rich edge (right in Fig. 3b) and a fuel-lean edge (left in Fig. 3b). The fuel-rich edge is indicated by the yellow flame in Fig. 2(b). Because the vortex is generated from different directions, the yellow flame in the edge occurs in various locations (see Video 2). Finally, a blue flame sheet is produced, probably because the regression in the middle produces a larger recirculation zone, as illustrated in Fig. 3(c). Numerical simulations with the Fire Dynamics Simulator (FDS) 6.5 [27] demonstrate these flame behavior (see Video 5). As a first approximation, the infinitely fast flame chemistry is assumed in the model, and combustion occurs right after mixing.

Further increasing the opposed flow velocity, the rotation of vortex becomes faster, and eventually, the flame is blown off. A critical strain rate (a^*) may be defined for blow-off as

$$a^* = \frac{U_a^*}{r} \tag{1}$$

where r is the radius of rod, and U_a^* is the blow-off flow velocity. Based on the blow-off flow velocity (also see Fig. 4), $a^* = 470 \pm 30$ s^{-1} is found for different sample sizes. More sophisticated numerical simulations with finite-rate chemistry are required to verify the proposed flame structures and critical strain rate.

3.3. Opposed flame spread and fuel regression

In these experiments, the motion of the flame is determined by tracking the flaming leading edge from the video frame by frame. The measured downward progress of the flame front or the "flame-spread rate" (V_f) in normal gravity under the opposed flow is summarized in Fig. 4 using both (a) normal and (b) logarithm coordinates. Similar experiments were conducted in the past [6], but the maximum opposed flow velocity tested was only 70 cm/s.

It is seen that the opposed flame spread rate is larger for smaller rod diameters. This is because of two reasons, (1) as the fuel is thinner the thermal inertia of the rods decrease and the heat transfer in the solid phase is also enhanced (2) the large curvature of the fuel surface enhances the convective heat flux from the flame [28].

Regarding the dependence of the spread rate on the flow velocity, when plotting the data in linear coordinates (Fig. 3a), for all rod diameters three different regions can be identified:

- In Region I (U_a < 30 cm/s), the applied forced flow is smaller than the flame-induced buoyant flow, so the flame spread is still controlled by the buoyant flow.
- In Region II (30 cm/s < U_a < 100 cm/s), the flame spread rate decreases quickly with the opposed flow velocity.
- In Region III (U_a > 100 cm/s), the "flame spread rate" is insensitive to the opposed flow velocity until extinction. The Region III was not observed in [6] because of the limited maximum flow velocity.

However, if the same data are plotted in the log-log coordinate (Fig. 4b), different trends between V_f and U_a are observed. Particularly, in the log-log coordinate the flame spread rate seems to (1) be "insensitive" to flow speed in Region I, and (2) change "significantly" in Region III. Therefore, caution is needed if presenting and analyzing the data in the log-log coordinate.

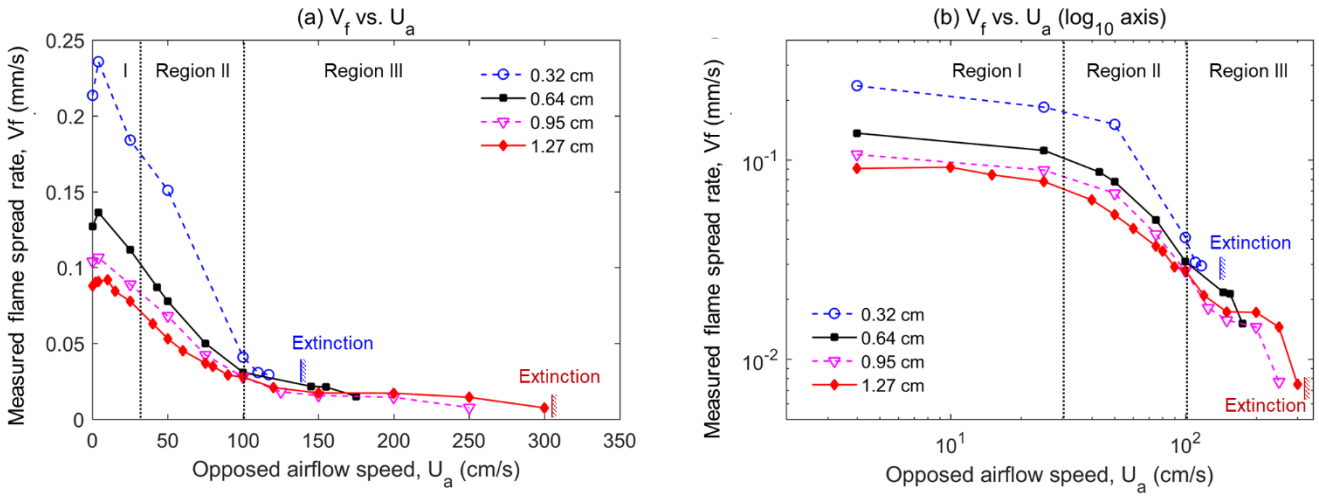

Fig. 4 Measured flame spread rate under opposed flow plotted in (a) normal axis, and (b) log10-log10 axis.

Different flame behaviors also reflect these different regions. The transition from Region II to III appears when the flame width decreases to the diameter of fuel (see Fig. 2a). In other words, the flame no longer spreads on the side of the fuel, but it moves downstream and hides in the recirculation zone above the fuel, which was also shown in numerical simulations [25]. Therefore, the observed "flame spread" is actually the motion of fuel regression, and it is very like a pool fire or a candle flame. In other words, the measured "flame-spread rate" is the fuel-regression rate in the vertical direction (R_v). Note that this "fuel-regression region" will not appear in thin rods, because above the fuel there is not enough space to have a recirculation zone. As seen from Fig. 4 and Eq. (1), as the rod diameter decreases, the fuel-regression region (Region III) becomes smaller, and flame is blown off at lower flow velocities.

Different Regions also show different shapes of the cone. Because the sample shape within the flame is not a perfect cone, there may be three characteristic angles to describe the shape of a cone, namely, cone angle (β), average regression angle (θ), and the leading-edge regression angle (α), as illustrated in Fig. 2(e). Measurement shows $\alpha < \theta$ when the angle is smaller than 30°, while $\alpha > \theta$ when the flow velocity becomes large. The average regression angle (θ) reflects the overall regression rate (or burning rate) and flame heat flux in the burning region. The cone angle (β) may indicate the local burning rate and flame heat flux at the tip of the cone. The value of β is

not only almost irrelevant to the flame spread behavior, but also difficult to determine when the tip is round and covered with the yellow flame, unless cutting the sample after experiment [21].

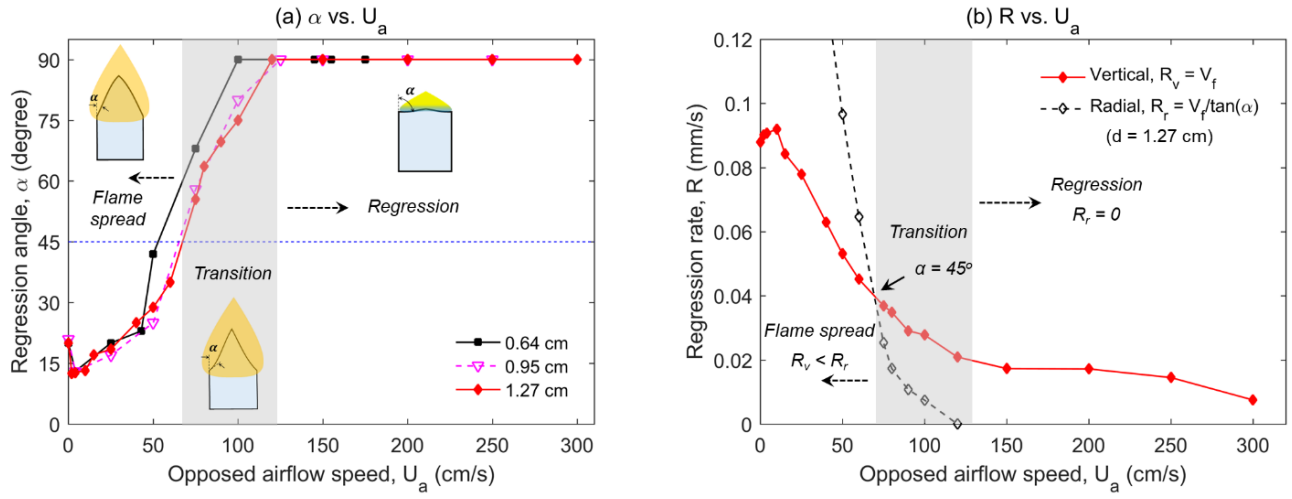

Fig. 5 (a) Fuel regression angle under varying opposed flow, and (b) regression rate in vertical direction ($R_v = V_f$) and radial direction ($R_r = V_f/\tan\alpha$).

On the other hand, the leading-edge regression angle (α) may quantify the local flame heat flux ($\dot{q}'' \approx \dot{m}''L$ [15]) and the regression rate ($R = \dot{m}''/\rho_f$) in the flame leading edge (or the preheating region), so it is most relevant to the flame spread. We can estimate that

$$\tan(\alpha) = \frac{R_v}{R_r} \approx \frac{\dot{q}_v''}{\dot{q}_r''} \tag{2}$$

where *v* and *r* represent the vertical and radial directions. Thus, the observed progress rate of the flame is the local regression rate in the vertical direction as

$$V_f = R_v = R\sin(\alpha) \tag{3}$$

Figure 5 shows (a) the leading-edge regression angle (α) as a function of the opposed flow velocity, and (b) the comparison of the fuel regression rate between vertical and radial directions (R_v vs. R_r). Based on the experimental observation, the transition from flame spread to fuel regression occurs at $\alpha \approx 45°$ and $U_a \approx 70$ cm/s. Further increasing the flow velocity above 100 cm/s, the edge of the top surface becomes flat (i.e. $\alpha = 90°$) until extinction, although there is still a smaller cone in the center of the top surface (Fig. 2a). Figure 5(b) further points out that the transition from flame spread to fuel regression occurs when the vertical regression rate is larger than the radial regression rate, i.e., $R_v > R_r$ or $\alpha > 45°$.

3.4. Reduced Pressure

Figure 6(a) shows the rate of flame spread and radial regression as a function of pressure. Both the rate of flame-spread and fuel-regression become slower at lower ambient pressure, and eventually, extinction occurs at a pressure lower than 15 kPa. As explained above, the flame width and flame standoff distance become larger at a lower pressure, so the convective heat flux from the flame to the solid is reduced. Figure 6(b) shows the measured leading-edge regression angle (α) as a function of pressure, where α increases as the pressure is decreased, i.e., the cone

becomes flatter. It is because the rate of regression in the radial direction ($R_r = V_f/\tan\alpha = R\cos\alpha$) is more sensitive to the pressure or to the convective heat flux, as compared with the flame spread rate V_f.

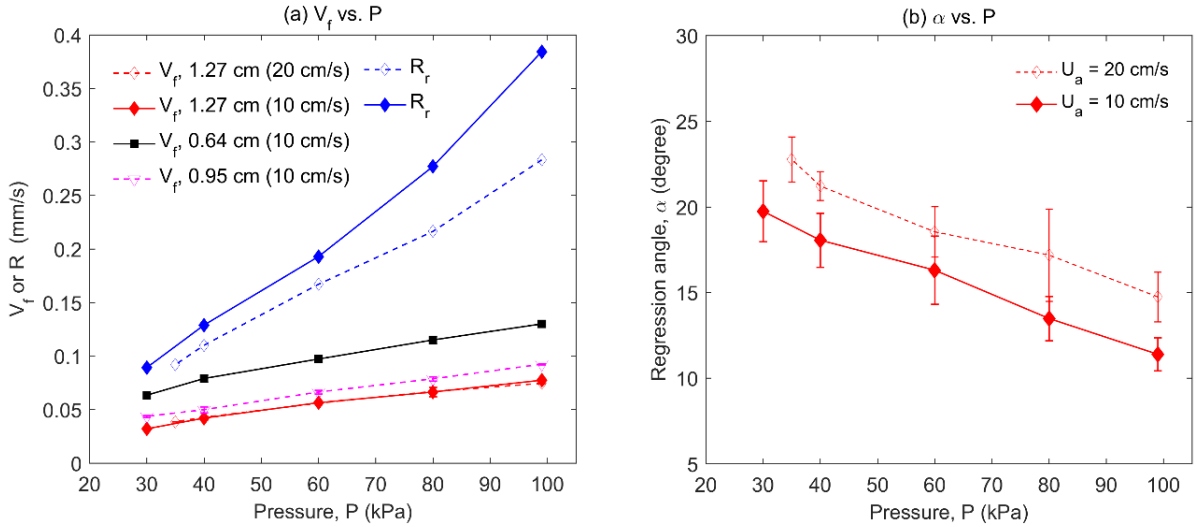

Fig. 6 (a) Flame spread rate and (b) regression angle (d = 1.27 cm) under reduced pressures.

Figure 6(b) also shows the combined effect of the opposed flow velocity and pressure on the regression angle. For example, the regression angle at an opposed flow of 20 cm/s and 100 kPa, is close to that at an opposed flow of 10 cm/s and 70 kPa. Thus, as the pressure decreases, the progress of the flame changes from flame-spread to fuel-regression at a smaller opposed flow velocity.

3.5. Oxygen concentration

As the O_2 concentration is decreased, the flame spread rate decreases due to the overall reduction in the flame heat flux (discussed more in [13]). Eventually, the flame will extinguish below the limiting oxygen concentration (LOC). Figure 7(a) shows the measured fuel regression angle (α) as a function of O_2 concentration. It is seen that the regression angle is extremely sensitive to the O_2 concentration for values smaller than 21%. Specifically, the flame quickly enters the fuel-regression region at 20% O_2 concentration, and the regression angle increases to 90° at 19% O_2 concentration. This result can be explained by the proposed transition criterion.

As the O_2 concentration decreases, the laminar burning velocity decreases significantly, so the transition from flame spread to fuel regression occurs at a much smaller opposed flow speed. Figure 7(b) shows that in lower O_2 concentration the flame becomes smaller as the cone is consumed gradually. A similar observation was previously made in [17]. Eventually, the flame is blown off by the opposed flow or the self-induced buoyant flow [13,29] (see Video 6). After extinction, the top surface of fuel residue is found to be flat, different from the surface depression found in 21% O_2 (Fig. 2b). In fact, at low O_2 concentration, the flat blue flame sheet in Fig. 2(b) is not observed. This is because the blow-off flow velocity is not large enough to generate the vortex street above the fuel.

Moreover, it also proves that in the ASTM limiting oxygen test [22], for a thick fuel, the flame is burning on the top surface, rather than spreading over the side, when the O_2 concentration approaches LOC. This also explains why different LOCs were found between thin and thick samples of the same material, as there is no stable recirculation zone for the thin fuel. Another exception is that if there are significant melting and dripping, the flame tends to attach to the dripping flow rather than burn in a stable recirculation zone, such as observed in [23,30].

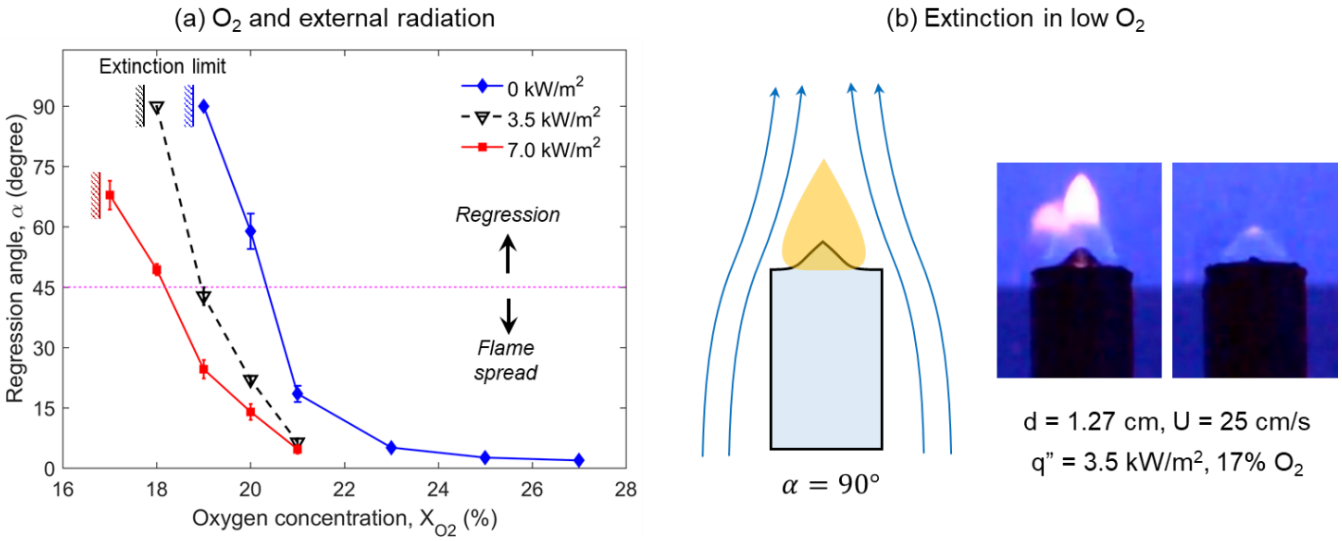

Fig. 7 (a) Fuel regression angle (α) under reduced O_2 concentration and external radiation, and (b) extinction in low O_2 concentration where the vortex street is not produced.

3.6. External radiation

When external radiation is applied from the radial direction (perpendicular to the flame-spread direction, see Fig. 1), the entire fire behavior change. Beside that the flame spread rate increases significantly with the external radiation, the flame can be sustained at a lower O_2 concentration (see Fig. 7). Quantitatively, as the external radiation increases from 0 to 7 kW/m^2, the LOC decreases from 18.5% to 16.5%.

Figure 7 also shows that the regression angle (α) decreases as the external radiation is increased. This trend could be explained by the increased flame spread rate because of the preheating of the solid ahead of the flame front. Also, the applied external radiation is in the radial direction which helps increase the overall heat flux in the radial direction ($\dot{q}_r''$), thus, decreasing the regression angle ($\tan(\alpha) \approx \dot{q}_v''/\dot{q}_r''$). For both reasons, applying the external radiation toward the preheating region prevents the extinction as well as the transition from flame spread to fuel regression. If the radiation is applied from the top (i.e. increasing $\dot{q}_v''$), a different trend may be observed for regression angle.

3.7. Microgravity

The microgravity experiments showed that as the opposed flow velocity is increased, the flame spread rate first increases, and then decreases, different from that in normal gravity. Figure 8(a) shows the regression angles of all tested PMMA rod samples in BASS-II microgravity experiments, which has the opposed flow velocity in the range of 0.4 and 7.6 cm/s. They are also compared to the regression angles from the normal-gravity experiments with a fixed opposed flow velocity of 4 cm/s under different O_2 concentrations. A previous analysis of the data [13] found that the opposed flame spread in microgravity could be faster and sustained at a lower O_2 concentration (17%) than in normal gravity (18%), as shown in Fig. 8(b) and discussed more in [13].

A very small regression angle ($\alpha \approx 5°$) is observed in the low-flow-velocity microgravity experiment, which is much smaller than that observed in normal gravity. Without the buoyant flow, the flame becomes shorter, blue, and concentric-cylinder like (Fig. 2d). Also, the flame does not cover and burnout the entire cone, probably because the overall flame heat flux decreases significantly due to the larger flame standoff distance (or the boundary layer thickness) and weaker flame. This has not been observed for PMMA in normal gravity before, because the strong

buoyant flow induced by flame, will either push the flame close to the fuel surface and increase the regression rate or blow off the flame if it is weak.

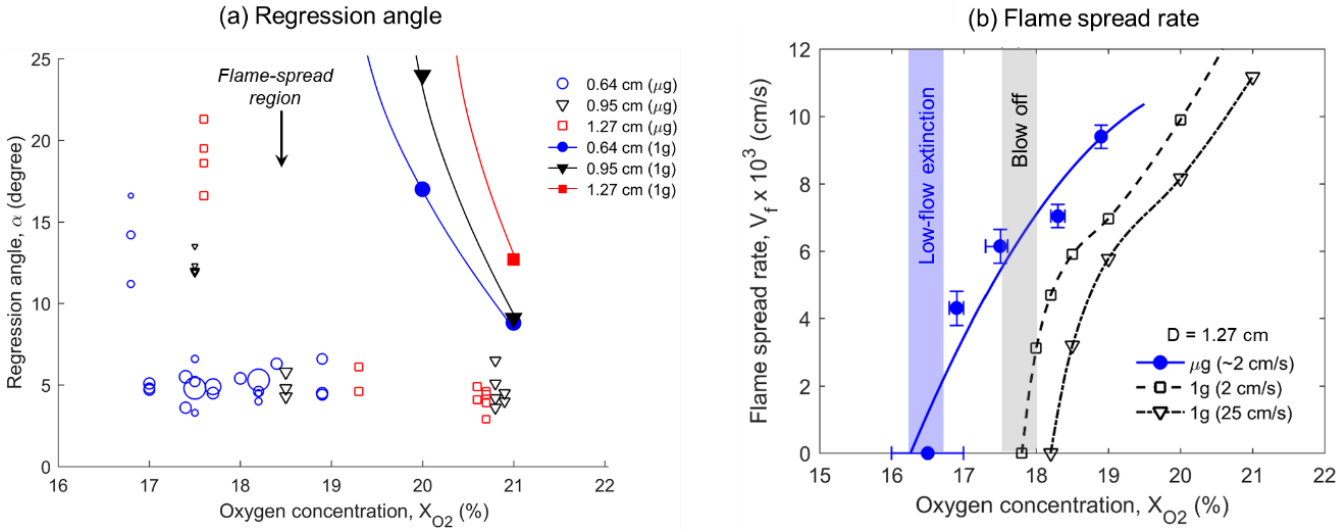

Fig. 8 (a) Fuel regression angle under microgravity and normal gravity, where the size of the symbol indicates the relative magnitude of the opposed flow velocity in the range of 0.4 and 7.6 cm/s, and (b) flame spread rate [13].

Because of the "floating concentric-cylinder flame" in microgravity, the flame heat flux in the vertical direction ($\dot{q}_v''$) decreases more significantly than $\dot{q}_r''$ in the radial direction, resulting in a smaller regression angle, $\alpha \approx \dot{q}_v''/\dot{q}_r''$. Figure 8(a) also shows that as the opposed flow velocity is further decreased to about 1 cm/s, there is also a clear increase in the regression angle, up to 22° before extinction. However, the regression angle never reaches the transition value of 45°. In other words, the flame is always spreading, and the fuel-regression region does not occur in microgravity under the low opposed flow velocity. It is also different from the two-step extinction process (i.e., first flame-spread to fuel-regression, and then blow-off) observed in normal gravity, as the opposed flow velocity increases gradually. Note that this two-step extinction process may also occur in microgravity under a larger opposed flow velocity. This needs to verify in future microgravity experiments with the longer experimental duration and longer fuels.

4. Conclusions

In this work, the flame spread and mass burning of cylindrical PMMA samples were conducted under varying opposed flow, pressure, O_2 concentration, external radiation, and gravity level (Earth and International Space Station). This work aims to systematically determine the transition between opposed flame spread and mass burning (or fuel regression).

Results show that in normal gravity, as the opposed flow increases to 50~100 cm/s, the flame can no longer spread over the fuel surface, but becomes a mass burning process, staying in the recirculation zone downstream of the cylinder top surface. Thus, the observed "flame-spread" is actually a fuel-regression like a pool fire flame or a candle flame. The fuel regression only occurs for the thick rods, but not for the thin rods which do not have a downstream recirculation zone. Such transition can also be indicated by a critical leading-edge regression angle of $\alpha \approx 45°$. Increasing the opposed flow velocity, the shape of cone becomes flatter until flame blow-off occurs. In

the present experiments, before blow-off, a flat blue flame is formed floating above the rod top surface, like a classical counterflow diffusion flame. Such blue flame is stable and is a result of vortex shedding.

As the ambient pressure or O_2 concentration decreases, the flame spread first transitions to the fuel regression regime, and then, extinction occurs (two-step extinction process). On the other hand, external radiation in the perpendicular to the flame-spread direction may prevent the transition to fuel regression if the radiant flux is elevated enough. In microgravity, the fuel regression angle is found to be much smaller ($<5^o$) in the low opposed flow (<10 cm/s) and the cone-shape fuel may not be formed after the flame spread, which is different from normal gravity. This work not only provides a better understanding of flame-spread and blow-off phenomena under various environmental conditions, but also clarify the differences between flame-spread and fuel-regression on solid fuels.

Acknowledgements

The authors would like to acknowledge the invaluable assistance of all the astronauts who ran BASS-II. This work could not have been done without the intense efforts of the BASS ops team (Jay Owens, Chuck Bunnell, Tibor Lorik, Carol Reynolds). We also want to acknowledge the ground support teams at GRC, JSC, MSFC that supported the BASS-II operations. This work was supported by NASA Grants NNX10AE01G and NNX13AL10A.

References

[1] F.A. Williams, Mechanisms of fire spread, Symposium (International) on Combustion. 16 (1977) 1281–1294. doi:10.1016/S0082-0784(77)80415-3.

[2] C.A. Fernandez-Pello, The solid phase, in: G. Cox (Ed.), Combustion Fundamentals of Fire, Academic Press INC., San Diego, 1995: pp. 31–100.

[3] C.R. Andracchio, T.H. Cochran, Gravity Effects on Flame Spreading over Solid Surfaces, NASA, 1977.

[4] T.J. Ohlemiller, K.M. Villa, Material Flammability Test Assessment for Space Station Freedom, 1991.

[5] J.N. De Ris, Spread of a laminar diffusion flame, Symposium (International) on Combustion. 12 (1969) 241–252. doi:10.1016/S0082-0784(69)80407-8.

[6] a. C. Fernandez-Pello, S.R. Ray, I. Glassman, Downward Flame Spread In an Opposed Forced Flow, Combustion Science and Technology. 19 (1978) 19–30. doi:10.1080/00102207808946860.

[7] A.C. Fernandez-Pello, S.R. Ray, I. Glassman, Flame spread in an opposed forced flow: the effect of ambient oxygen concentration, Symposium (International) on Combustion. 18 (1981) 579–589. doi:10.1016/S0082-0784(81)80063-X.

[8] A.E. Frey, J.S. T'ien, A theory of flame spread over a solid fuel including finite-rate chemical kinetics, Combustion and Flame. 36 (1979) 263–289. doi:10.1016/0010-2180(79)90064-6.

[9] I.S. Wichman, Theory of opposed-flow flame spread, Progress in Energy and Combustion Science. 18 (1992) 553–593. doi:10.1016/0360-1285(92)90039-4.

[10] S.L. Olson, P. V Ferkul, S. Bhattacharjee, F.J. Miller, A.C. Fernandez-Pello, J.S. T'ien, Burning and Suppression of Solids – II Fire Safety Investigation for the Microgravity Science Glovebox, 29th Annual Meeting of the American Society for Gravitational and Space Research (ASGSR) and the 5th International Symposium on Physical Sciences in Space (ISPS). (2013).

[11] S. Bhattacharjee, A. Simsek, F. Miller, S. Olson, P. Ferkul, Radiative, thermal, and kinetic regimes of opposed-flow flame spread: A comparison between experiment and theory, Proceedings of the Combustion Institute. 36 (2017) 2963–2969. doi:10.1016/j.proci.2016.06.025.

[12] S.L. Olson, P. V. Ferkul, Microgravity flammability boundary for PMMA rods in axial stagnation flow: Experimental results and energy balance analyses, Combustion and Flame. 180 (2017) 217–229. doi:10.1016/j.combustflame.2017.03.001.

[13] S. Link, X. Huang, C. Fernandez-Pello, S. Olson, P. Ferkul, The Effect of Gravity on Flame Spread over PMMA Cylinders, Scientific Reports. 8 (2018) 120. doi:10.1038/s41598-017-18398-4.

[14] M.A.D. Robert A. Altenkirch, Lin Tang, Kurt Sacksteder, Subrata Bhattacharjee, R.A. Altenkirch, L. Tang, K. Sacksteder, S. Bhattacharjee, M.A. Delichatsios, Inherently unsteady flame spread to extinction over thick fuels in microgravity, Proceedings of the Combustion Institute. 27 (1998) 2515–2524. doi:10.1016/S0082-0784(98)80103-3.

[15] J.G. Quintiere, Fundamentals of fire phenomena, John Wiley, 2006. doi:10.1002/0470091150.

[16] M. Sibulkin, C.K. Lee, Flame Propagation Measurements and Energy Feedback Analysis for Burning Cylinders, Combustion Science and Technology. 9 (1974) 137–147. doi:10.1080/00102207408960349.

[17] M. Sibulkin, M.W. Little, Propagation and Extinction of Downward Burning Fires, Combustion and Flame. 31 (1978) 197–208. doi:10.1016/0010-2180(78)90129-3.

[18] A. Kumar, J.S. T'ien, A computational study of low oxygen flammability limit for thick solid slabs, Combustion and Flame. 146 (2006) 366–378. doi:10.1016/j.combustflame.2006.02.008.

[19] M.J. Gollner, X. Huang, J. Cobian, A.S. Rangwala, F.A. Williams, Experimental study of upward flame spread of an inclined fuel surface, Proceedings of the Combustion Institute. 34 (2013) 2531–2538. doi:10.1016/j.proci.2012.06.063.

[20] Y. Kobayashi, X. Huang, S. Nakaya, M. Tsue, C. Fernandez-Pello, Flame Spread over Wires: the Role of Dripping and Core, Fire Safety Journal. 91 (2017) 112–122. doi:10.1016/j.firesaf.2017.03.047.

[21] L. Carmignani, B. Rhoades, S. Bhattacharjee, Correlation of Burning Rate with Spread Rate for Downward Flame Spread Over PMMA, Fire Technology. 54 (2018) 1–12. doi:10.1007/s10694-017-0698-3.

[22] ASTM, Standard Test Method for Measuring the Minimum Oxygen Concentration to Support Candle-Like Combustion of Plastics (Oxygen Index), 2010. doi:10.1520/D2863-12.1.

[23] K. Miyamoto, X. Huang, N. Hashimoto, O. Fujita, C. Fernandez-Pello, Limiting Oxygen Concentration (LOC) of Burning Polyethylene Insulated Wires under External Radiation, Fire Safety Journal. 86 (2016) 32–40. doi:10.1016/j.firesaf.2016.09.004.

[24] M. Thomsen, D.C. Murphy, C. Fernandez-pello, D.L. Urban, G.A. Ruff, Flame spread limits (LOC) of fire resistant fabrics, Fire Safety Journal. 91 (2017) 259–265. doi:10.1016/j.firesaf.2017.03.072.

[25] A. Fuentes, G. Legros, A. Claverie, P. Joulain, J.P. Vantelon, J.L. Torero, Interactions between soot and CH* in a laminar boundary layer type diffusion flame in microgravity, Proceedings of the Combustion Institute. 31 II (2007) 2685–2692. doi:10.1016/j.proci.2006.08.031.

[26] K.M. Lyons, Toward an understanding of the stabilization mechanisms of lifted turbulent jet flames: Experiments, Progress in Energy and Combustion Science. 33 (2007) 211–231. doi:10.1016/j.pecs.2006.11.001.

[27] K. McGrattan, S. Hostikka, R. McDermott, J. Floyd, C. Weinschenk, K. Overholt, FDS technical reference guide volume 1 : Mathematical Model, 2017. doi:10.6028/NIST.SP.1018-1.

[28] M.A. Delichatsios, R.A. Altenkirch, M.F. Bundy, S. Bhattacharjee, L. Tang, K. Sacksteder, Creeping flame spread along fuel cylinders in forced and natural flows and microgravity, Proceedings of the Combustion Institute. 28 (2000) 2835–2842. doi:10.1016/S0082-0784(00)80706-7.

[29] M.C. Johnston, J.S. T'Ien, D.E. Muff, X. Zhao, S.L. Olson, P. V. Ferkul, Self induced buoyant blow off in upward flame spread on thin solid fuels, Fire Safety Journal. 71 (2015) 279–286. doi:10.1016/j.firesaf.2014.11.007.

[30] Y. Nakamura, K. Kizawa, S. Mizuguchi, A. Hosogai, K. Wakatsuki, Experimental Study on Near-Limiting Burning Behavior of Thermoplastic Materials with Various Thicknesses Under Candle-Like Burning Configuration, Fire Technology. 52 (2016) 1–25. doi:10.1007/s10694-016-0567-5.